



# CHORUS

This is the accepted manuscript made available via CHORUS. The article has been published as:

## Ultrahigh-energy cosmic ray composition from the distribution of arrival directions

Rita C. dos Anjos, Jorge F. Soriano, Luis A. Anchordoqui, Thomas C. Paul, Diego F. Torres, John F. Krizmanic, Timothy A. D. Paglione, Roberto J. Moncada, Frederic Sarazin, Lawrence Wiencke, and Angela V. Olinto

Phys. Rev. D **98**, 123018 — Published 26 December 2018

DOI: [10.1103/PhysRevD.98.123018](https://doi.org/10.1103/PhysRevD.98.123018)

# Ultrahigh-Energy Cosmic Ray Composition from the Distribution of Arrival Directions

Rita C. dos Anjos,<sup>1,2</sup> Jorge F. Soriano,<sup>1,3</sup> Luis A. Anchordoqui,<sup>1,3,4</sup> Thomas C. Paul,<sup>1</sup>  
Diego F. Torres,<sup>5,6,7</sup> John F. Krizmanic,<sup>8</sup> Timothy A. D. Paglione,<sup>3,4,9</sup>  
Roberto J. Moncada,<sup>4,10</sup> Frederic Sarazin,<sup>11</sup> Lawrence Wiencke,<sup>11</sup> and Angela V. Olinto<sup>12,13</sup>

<sup>1</sup>Department of Physics & Astronomy, Lehman College, City University of New York, NY 10468, USA

<sup>2</sup>Departamento de Engenharias e Exatas, Universidade Federal do Paraná, 85950-000 Palotina, Brazil

<sup>3</sup>Department of Physics, Graduate Center, City University of New York, NY 10016, USA

<sup>4</sup>Department of Astrophysics, American Museum of Natural History, NY 10024, USA

<sup>5</sup>Institute of Space Sciences (ICE-CSIC), Campus UAB, Carrer de Magrans s/n, 08193 Barcelona, Spain

<sup>6</sup>Institució Catalana de Recerca i Estudis Avançats (ICREA), E-08010 Barcelona, Spain

<sup>7</sup>Institut d'Estudis Espacials de Catalunya (IEEC), 08034 Barcelona, Spain

<sup>8</sup>NASA Goddard Space Flight Center, Greenbelt, MD, USA

<sup>9</sup>Department of Earth & Physical Sciences, York College, City University of New York, NY 11451, USA

<sup>10</sup>Department of Physics, University of Miami, Coral Gables, FL 33146, USA

<sup>11</sup>Department of Physics, Colorado School of Mines, Golden, CO 80401, USA

<sup>12</sup>Department of Astronomy & Astrophysics, University of Chicago, Chicago, IL 60637, USA

<sup>13</sup> Enrico Fermi Institute and Kavli Institute for Cosmological Physics, University of Chicago, Chicago, IL 60637, USA

The sources of ultrahigh-energy cosmic rays (UHECRs) have been difficult to catch. It was recently pointed out that while sources of UHECR protons exhibit anisotropy patterns that become denser and compressed with rising energy, nucleus-emitting-sources give rise to a *cepa stratis* (onion-like) structure with layers that become more distant from the source position with rising energy. The peculiar shape of the hot spots from nucleus-accelerators is steered by the competition between energy loss during propagation and deflection on the Galactic magnetic field (GMF). Here, we run a full-blown simulation study to accurately characterize the deflections of UHECR nuclei in the GMF. We show that while the *cepa stratis* structure provides a global description of anisotropy patterns produced by UHECR nuclei *en route* to Earth, the hot spots are elongated depending on their location in the sky due to the regular structure of the GMF. We demonstrate that with a high-statistics sample at the high-energy-end of the spectrum, like the one to be collected by NASA's POEMMA mission, the energy dependence of the hot-spot contours could become a useful observable to identify the nuclear composition of UHECRs. This new method to determine the nature of the particle species is complementary to those using observables of extensive air showers, and therefore is unaffected by the large systematic uncertainties of hadronic interaction models.

## I. INTRODUCTION

The search for the sources of ultrahigh-energy cosmic rays (UHECRs) continues to be one of the most challenging and at the same time most important tasks in astrophysics [1, 2]. UHECR deflection by intervening magnetic fields hampers pinning down their origins. The most recent data (interpreted using various hadronic models) seem to indicate that the most energetic ( $E \gtrsim 10^{10}$  GeV) cosmic rays may not just be protons, but rather atomic nuclei of charge  $Ze$  [3–6]. Even though cosmic ray trajectories would naturally undergo less magnetic bending as the kinetic energy (rigidity) is increased, UHECR nuclei are expected to suffer significant deflections while traversing the Galaxy.

To make things worse, magnetic fields are not well constrained by current data. If we endorse recent models of the Galactic magnetic field (GMF) [7–10], then typical values of the deflections of UHECRs crossing the Galaxy are

$$\theta \sim 10^\circ Z \left( \frac{E}{10^{10} \text{ GeV}} \right)^{-1}, \quad (1)$$

depending on the direction considered [11, 12]. Therefore, tracing the origin of a particular UHECR nucleus

back to its source in the sky is not trivial.

UHECR nuclei lose energy *en route* to Earth through interactions with the universal radiation fields [13–15]. Thus and so, it was recently pointed out that the combination of magnetic deflections and energy losses during propagation should produce an unequivocal anisotropy pattern for accelerators of UHECR nuclei: a *cepa stratis* structure with layers that increase with rising energy [16]. This is in sharp contrast to anisotropy patterns of pure-proton sources, which become denser and compressed with rising energy. The combination of these effects leads to an onion-like layered structure depending on composition and energy. To visualize this, first recall that if the sources emitted only protons, the size of the corresponding “spot” should decrease with rising energy due to reduced deflection in magnetic fields. In contrast, if sources produce a mixed composition, a different quality emerges. Lighter compositions tend to shorter mean-free-paths at higher energies, so as their energy increases they begin to disappear from the sample leaving behind only the lower energy component. The latter suffers a relatively smaller magnetic deflection compared to heavier nuclei at all energies. One thus ends up with a *cepa stratis* structure in which the energies of the species observed closer to the source

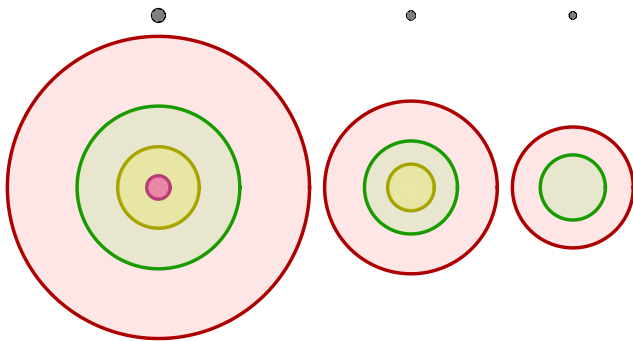


FIG. 1: Circles representing the composition-layered structure of hotspots at different energies, for proton sources (top) and nuclei sources (bottom). The radii of the circles respect the proportions of the angular sizes given by (1), for protons (black), helium (magenta), nitrogen (yellow), silicon (green) and iron (red); and for 40 EeV (left), 70 EeV (center) and 100 EeV (right).

have a *lower* rather than higher energy, as they would in the case that the sources emitted only protons. This effect is shown schematically in Fig. 1.

In this paper we simulate realistic UHECR sky maps for a wide range of possible nuclear species and study individual anisotropy patterns from nearby sources to quantify the variation in (shape and size) of the expected “squeezed onion layers.” We also present a statistical test to isolate the UHECR nuclear composition using a subsample of the distribution of arrival directions associated with a particular source in the cosmic-ray-sky. All source types are represented within our cosmic backyard for light and heavy nuclei, so all source types are *a priori* candidates for the nearby exploration.

The layout of the paper is as follows. We begin in Sec. II with an overview of the main characteristics of potential nearby sources. In Sec. III we study the energy losses during propagation and in Sec. IV the deflections on the GMF. Armed with our findings, in Sec. V we develop a statistical test to probe the nuclear composition of UHECR using the distribution of arrival directions. After that, in Sec. VI we demonstrate that NASA’s Probe Of Extreme Multi-Messenger Astronomy (POEMMA) mission [17] will attain sensitivity to clarify the nuclear composition of recently reported hot spots by the Telescope Array and Pierre Auger collaborations [18]. The paper wraps up with some conclusions presented in Sec. VII.

## II. EXPERIMENTAL DATA

### A. UHECR Anisotropies

Over the years, stronger and stronger experimental evidence has been accumulating indicating a possible

correlation between the arrival directions of the highest energy cosmic rays and nearby starburst galaxies [19, 20]. Recently, using data collected by the Pierre Auger Observatory, the hypothesis of UHECR emission from the 23 brightest nearby starburst galaxies (SBGs) with a radio flux larger than 0.3 Jy (selected out the 63 objects within 250 Mpc search for gamma-ray emission by the Fermi-LAT Collaboration [21]) was tested against the null hypothesis of isotropy through an unbinned maximum-likelihood analysis [20]. The adopted test statistic (TS) for deviation from isotropy being the standard likelihood ratio test between the starburst-generated UHECR sky model and the null hypothesis. The TS was maximized as a function of two free parameters (the angular radius common to all sources, which accounts in an effective way for the magnetic deflections, and the signal fraction), with the energy threshold varying in the range  $10^{10.3} \lesssim E/\text{GeV} \lesssim 10^{10.9}$ . For a given energy threshold, the TS for isotropy follows a  $\chi^2$  distribution with two degrees of freedom. The TS is maximum above  $10^{10.6}$  GeV, with a local *p*-value of  $3 \times 10^{-6}$ . The smearing angle and the anisotropic fraction corresponding to the best-fit parameters are  $13_{-3}^{+4}$  and  $(10 \pm 4)\%$ , respectively. Remarkably, the energy threshold of largest statistical significance coincides with the observed suppression in the spectrum [22–24], implying that when we properly account for the barriers to UHECR propagation in the form of energy loss mechanisms [13, 14] we obtain a self consistent picture for the observed UHECR horizon. The scan in energy thresholds comes out with a penalty factor, which was estimated through Monte-Carlo simulations. The post-trial chance probability in an isotropic cosmic ray sky is  $4.2 \times 10^{-5}$ , corresponding to a 1-sided Gaussian significance of  $4\sigma$  [20].

Auger data ( $E \gtrsim 10^{10.77}$  GeV) also show a slightly weaker association ( $2.7\sigma$ ) with active galactic nuclei (AGNs) that emit  $\gamma$ -rays (a.k.a.  $\gamma$ AGNs) from the 2nd catalogue of hard *Fermi*-LAT sources (2FHL) [25]. The maximum deviation for  $\gamma$ AGNs is found at an intermediate angular scale of  $7_{-2}^{+4}$  with an anisotropic fraction of  $(7 \pm 4)\%$  [20].

On a separate track, the Telescope Array (TA) has recorded a statistically significant excess in cosmic rays, with energies above  $10^{10.75}$  GeV, above the isotropic background-only expectation [26, 27]. This is colloquially referred to as the “TA hot spot.” The excess is centered at Galactic coordinates  $(l, b) \simeq (177^\circ, 50^\circ)$ , spanning a region of the sky with  $\sim 20^\circ$  radius. The chance probability of this hot spot in an isotropic cosmic ray sky was calculated to be  $3.7 \times 10^{-4}$ , corresponding to  $3.4\sigma$ .

The most recent search for hot spot anisotropies is a joint effort by the two collaborations considering 840 events recorded by Auger with  $E > E_{\text{Auger}} = 10^{10.6}$  GeV and 130 events recorded by TA with  $E > E_{\text{TA}} = 10^{10.73}$  GeV [18]. Before proceeding, we pause to note that though the techniques for assigning energies to events are nearly the same in both experiments, there are differences as to how the primary energies are derived at

Auger and TA, with systematic uncertainties in the energy scale of the experiments amounting to about 14% and 21% respectively, corresponding to about 70% uncertainty in the flux above a fixed energy threshold. By comparison, the uncertainties on the respective exposures are minor ( $\lesssim 1\%$  and  $\approx 3\%$ , respectively). Therefore, it is necessary to cross-calibrate the energy scales of the two datasets to avoid introducing a spurious North/South asymmetry due to an energy scale mismatch. This is accomplished by exploiting the wide declination band ( $-16^\circ \lesssim \delta \lesssim +45^\circ$ ) where the two datasets overlap. Regardless of the true arrival direction distribution, within a region of the sky  $\Delta\Omega$  fully contained in the field of view (FoV) of both observatories, the sum over observed events  $\sum_i 1/\omega(\mathbf{n}_i)$  (where  $\omega$  is the directional exposure of each observatory in the direction  $\mathbf{n}_i$ , in km yr units) is an unbiased estimator of  $\int_{\Delta\Omega} \Phi(\mathbf{n}) d\mathbf{n}$  (where  $\Phi$  is the directional UHECR flux integrated above the considered energy threshold, in  $\text{km}^{-2} \text{yr}^{-1} \text{sr}^{-1}$  units) and should be the same for both experiments except for statistical fluctuations. This criterium is generally adopted to cross-calibrate the energy scales and to determine  $E_{\text{Auger}}$  and  $E_{\text{TA}}$  such that the Auger flux above  $E_{\text{Auger}}$  matches the TA flux above  $E_{\text{TA}}$  [28].<sup>1</sup> The most significant excesses observed in a  $20^\circ$  search are at right ascensions and declinations:  $(\alpha, \delta) \approx (303.0^\circ, 12.9^\circ)$  and  $(\alpha, \delta) \approx (162.5^\circ, 44.4^\circ)$ , with local (Li-Ma [29]) statistical significance for the rejection of the null (background only) hypothesis of  $4.7\sigma$  and  $4.2\sigma$ , respectively [18]. The Li-Ma significance map of this data-sample is shown in Fig. 2. The most significant hot spot is near the location of starburst galaxies NGC 4945 and M83. The possible association of the TA hot spot with M82 has not gone unnoticed [31–35]. A warm spot is also visible in the vicinity of NGC 253 near the Galactic south pole.

Very recently, the TA Collaboration carried out a test of the reported correlation between the arrival directions of UHECRs and SBGs [20]. The data sample for this analysis includes cosmic rays with  $E > E'_{\text{TA}} = 43 \text{ EeV}$  detected by TA in a nine year period from May 2008 to May 2017. These data are compatible with isotropy to within  $1.1\sigma$  and with Auger result to within  $1.4\sigma$ , and so the TA Collaboration concluded that with their current statistics they cannot make a statistically significant corroboration or refutation of the reported possible correlation between UHECRs and SBGs [36]. It is important to note, however, that  $E'_{\text{TA}} < E_{\text{TA}}$ . Most importantly,  $E_{\text{TA}}$  is above the energy at which TA observes the suppression in the spectrum [37, 38], but  $E'_{\text{TA}}$  is below. This implies that the data sample of the test carried out by the TA Collab-

TABLE I: Spectral indices of selected nearby sources:  $\gamma$  maximizes the likelihood and  $[\gamma_l, \gamma_r]$  indicates to a 68% confidence interval of the spectral index.

Source	Dataset	Events	$\gamma$	$\gamma_l$	$\gamma_r$
NGC 253	Auger	8	4.8	3.6	6.4
NGC 4945	Auger	14	6.8	5.4	8.5
M83	Auger	13	4.6	3.7	5.7
NGC 1068	Auger	8	4.9	3.7	6.4
NGC 1068	TA	2	3.9	2.3	6.5
M82	TA	3	5.3	3.3	8.3
Cen A	Auger	16	5.5	4.5	6.8
Fornax A	Auger	7	7.0	5.0	9.5
M87	Auger	3	15.2	8.5	25.0
M87	TA	2	8.7	4.5	15.5

oration is most likely contaminated from the isotropic background of UHECRs emitted by far away sources, and consequently this would tend to reduce the significance of any possible correlation with nearby sources.

## B. Source Spectra

It has long been suspected that the powerful jets and the mammoth radio-lobes of nearby  $\gamma$ AGNs [39, 40] as well as the galactic-scale superwinds of SBGs [41] provide profitable arenas for the formation of collisionless plasma shock waves, in which UHECRs can be accelerated by bouncing back and forth across the shock. In addition, because of the high prevalence of supernovae, SBGs are thought to contain a large density of newly-born pulsars, which can accelerate UHECRs via unipolar induction [42, 43].

Arguably, when all of the above is combined  $\gamma$ AGNs and SBGs become the leading candidate sources at the very high energy end of the spectrum. Therefore, we will adopt these astrophysical objects as our working example.

In order to describe the sources properly, we study the spectra of Auger and TA events around selected objects that are relevant for this analysis. We consider the data published in [26, 44], consisting on 231 events above 52 EeV detected by the Pierre Auger Observatory, and 72 events above 57 EeV detected by TA. We select several sources from Auger and TA searches of anisotropy. For each of those sources, we define an angular window around their directions on the sky with angular radius of  $15^\circ$ , as shown in Fig. 3. This value serves just as an orientation, and we do not imply that the events from those sources should be contained in those angular windows. Nevertheless, the analysis presented in [44] results in such angular size for one of the sources. We perform a maximum likelihood estimation of the spectral index around each of the sources, for each of the data samples (if there is more than one event), assuming a single

<sup>1</sup> Actually, the region of the sky which is mostly used spans the declination band  $-12^\circ \leq \delta \leq +42^\circ$ . This is because including directions too close to the edge of the FoV of one of the observatories would result in larger statistical fluctuations due to very large values of  $1/\omega(\mathbf{n}_i)$  near the edge.

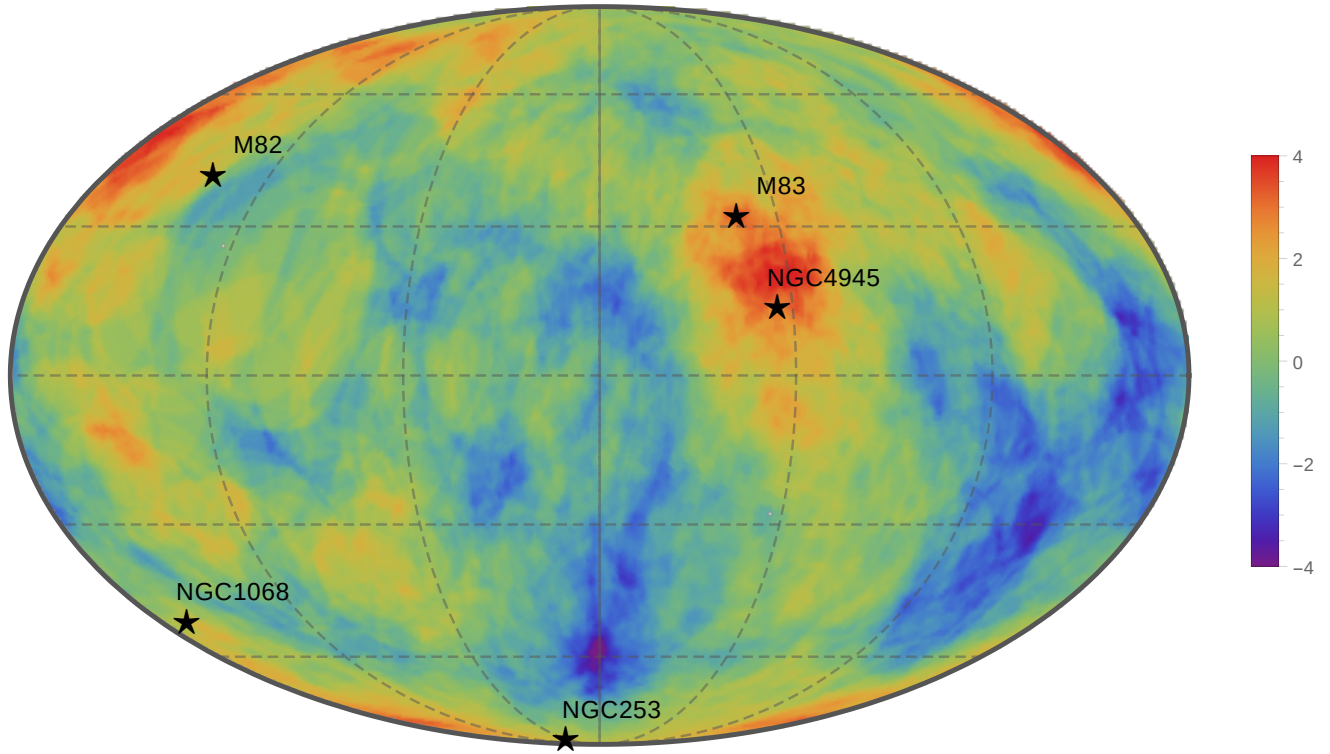


FIG. 2: Skymap in Galactic coordinates of the Li-Ma significances of overdensities in  $20^\circ$  radius windows for 840 events recorded by Auger with  $E > E_{\text{Auger}}$  and 130 events recorded by TA with  $E > E_{\text{TA}}$  [30]. The color scale indicates the significance in units of standard deviations; negative values follow the convention of indicating the (positive) significance of deficits.

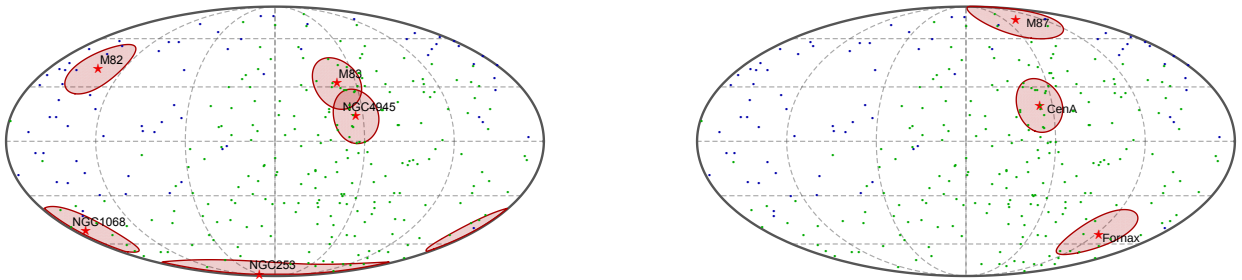


FIG. 3: Comparison of UHECR event locations with starburst- (left) and radio-galaxies (right) in Galactic coordinates. The green points indicate the arrival directions of 231 events with  $E > 52$  EeV and zenith angle  $\theta < 80^\circ$  detected by the Pierre Auger Observatory from 2004 January 1 up to 2014 March 31 [44]. The blue points indicate the arrival directions of 72 events with  $E > 57$  EeV and  $\theta < 55^\circ$  recorded from 2008 May 11 to 2013 May 4 with TA [22]. The stars indicate the location of nearby starburst- (left) and radio-galaxies (right). The shaded regions delimit angular windows around the sources of angular radius of  $15^\circ$ .

power law spectrum,  $dN/dE \propto E^{-\gamma}$ . In Table I we show the values of  $\gamma$  maximizing the likelihood, as well as the 68% confidence level intervals  $[\gamma_l, \gamma_r]$ . All the individual spectra are very steep, reflecting the suppression in the nearly isotropic UHECR spectrum.

### C. Starburst Energetics

It was recently pointed out that starburst superwinds struggle to meet the power requirements to accelerate cosmic rays to the maximum observed energies [45]. In detail, the magnetic field  $B$  carries with it an energy density  $B^2/(8\pi)$  and the flow carries with it an energy flux  $> uB^2/(8\pi)$ , where  $u$  is the shock velocity. Thus, for an



accelerator of size  $R$ , this sets a lower limit on the rate at which the energy is carried by the out-flowing plasma,

$$L_B > \frac{1}{8} u R^2 B^2, \quad (2)$$

and which must be provided by the source [46]. Inserting typical parameters of SBGs ( $L_B \sim 10^{42.5}$  erg/s,  $R \sim 8$  kpc, and  $u \sim 10^{3.3}$  km/s [47]) into (2) leads to the constraint  $B < 15 \mu\text{G}$ , and consequently a Hillas maximum rigidity

$$\mathcal{R} \simeq (u/c) B R < 10^{8.9} \text{ GV}. \quad (3)$$

However, radio continuum and polarization observations of M82 provide an estimate of the magnetic field strength in the core region of  $98 \mu\text{G}$  and in the halo of  $24 \mu\text{G}$ ; see e.g. the equipartition  $B$  map in Fig. 16 of [48]. Averaging the magnetic field strength over the whole galaxy results in a mean equipartition field strength of  $35 \mu\text{G}$ . Independent magnetic field estimates from polarized intensities and rotation measures yield similar strengths [49]. Comparable field strengths have been estimated for NGC 253 [50–53] and other starbursts [54]. Actually, the field strengths could be higher if the cosmic rays are not in equipartition with the magnetic field [55, 56]. In particular, mG magnetic field strengths have been predicted [57] and measured [58] in the starburst core of Arp 220. The cosmic ray population in the starburst is dominated by the nearest accelerators in time/space to the position of interest, thus breaking a direct relation between average fields and mean cosmic ray population [59]. Up to mG field strengths are consistent with the gamma-ray and radio spectra in the gas-rich starburst cores of NGC 253 and M82 [60]. Besides, the field strength in the halo of M82 and NGC 253 could be as high as  $300 \mu\text{G}$  [61–63]. Herein we will remain agnostic with regard to the process responsible for magnetic field amplification, and we consider all the nearby AGN and SBG sources which are consistent with Auger and TA observations.

### III. NUCLEUS PHOTODISINTEGRATION

The mean free path (mfp) for the different elements is obtained from the photodisintegration cross section and the background photon flux (of type  $k$ ) as

$$\frac{1}{\lambda_k} = \frac{1}{2\gamma^2} \int_{\varepsilon_{\text{th}}/2\gamma}^{\infty} \frac{1}{\varepsilon^2} f_k(\varepsilon) d\varepsilon \int_{\varepsilon_{\text{th}}}^{2\gamma\varepsilon} \varepsilon' \sigma_A(\varepsilon') d\varepsilon', \quad (4)$$

where  $\varepsilon_{\text{th}}$  is the threshold energy for the reaction in the nucleus rest frame,  $\gamma$  is the relativistic factor for the nucleus, and  $f_k$  is the photon distribution function (number of photons per unit volume and energy) in the frame where the cosmic microwave background (CMB) is at 2.7 K, in which it is assumed to be isotropic [64]. With a change of variables  $\varepsilon \rightarrow \varepsilon/2\gamma$  we can rewrite (4) as

$$\frac{1}{\lambda_k} = \frac{1}{\gamma} \int_{\varepsilon_{\text{th}}}^{\infty} \frac{1}{\varepsilon^2} f_k \left( \frac{\varepsilon}{2\gamma} \right) I(\varepsilon) d\varepsilon, \quad (5)$$

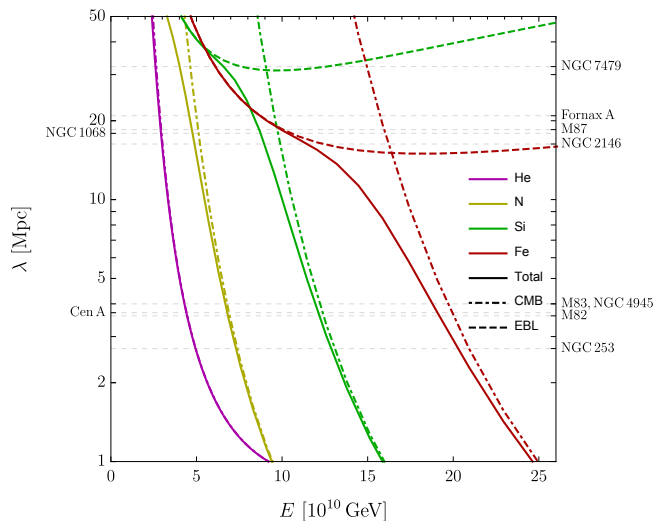


FIG. 4: Photodisintegration mfp on the CMB and EBL. The horizontal dashed lines indicate the distance to nearby starbursts and radio galaxies.

where

$$I(\varepsilon) \equiv \int_{\varepsilon_{\text{th}}}^{\varepsilon} \varepsilon' \sigma_A(\varepsilon') d\varepsilon'. \quad (6)$$

For nitrogen, silicon and iron, the cross section is taken from TALYS 1.8 as done by CRPropa3 [65], where the parameters of the giant dipole resonance (GDR) are modified according to the IAEA atlas, which show a better agreement with experimental data. For helium, the cross section is taken from Eq. (3) in [66]. The relevant photon backgrounds are the extragalactic background light (EBL) and the CMB. For the CMB, we take

$$f_{\text{CMB}} = \frac{1}{(hc)^3} \left( \frac{\varepsilon}{\pi} \right)^2 \left[ e^{\varepsilon/T} - 1 \right]^{-1}, \quad (7)$$

corresponding to a Bose-Einstein distribution with temperature  $T = 2.7255(6)$  K [67]. For the EBL, we take the results from [68].

In Fig. 4 we show the photodisintegration mfp for various nuclei. It is evident that the mfp decreases rapidly with increasing energy, and increases rapidly with increasing nuclear composition. More precisely,

- at  $E = 10^{10.7}$  GeV, the mfp for ionized helium ( $^4\text{He}$ ) is about 3 Mpc, while at  $10^{10.9}$  GeV it is nil;
- at  $E = 10^{10.9}$  GeV, the mfp for ionized nitrogen ( $^{14}\text{N}$ ) is about 4 Mpc, while at  $10^{11}$  GeV it is nil;
- at  $E = 10^{11.1}$  GeV, the mfp for ionized silicon ( $^{28}\text{Si}$ ) is about 2.5 Mpc, while at  $10^{11.2}$  GeV it is nil;
- until finally we reach ionized iron ( $^{56}\text{Fe}$ ) where the mfp at  $E = 10^{11.3}$  GeV is about 4 Mpc, while at  $10^{11.4}$  GeV it too is nil.

TABLE II: Energy cutoff  $E_A(D)$  for various nuclear species.

$D/\text{Mpc}$	$E_4/\text{EeV}$	$E_{14}/\text{EeV}$	$E_{28}/\text{EeV}$	$E_{56}/\text{EeV}$
2 to 3	60	100	180	220
3 to 4	50	80	130	210
16 to 21	40	60	100	110

This implies that from sources at increasing distance, fewer and heavier nuclei at highest energies are expected to reach Earth. The main features in the energy evolution of the abundance of various nuclear species on Earth can be summarized as follows:

- the contribution of  ${}^4\text{He}$  should decrease with rising energy and then essentially disappear above about  $10^{10.8}$  GeV;
- on average, only species heavier than  ${}^{14}\text{N}$  can contribute to the observed flux on Earth above  $10^{11}$  GeV, with nuclear species lighter than  ${}^{28}\text{Si}$  highly suppressed at  $10^{11.2}$  GeV;
- the mean flux of iron nuclei becomes suppressed somewhat below  $10^{11.4}$  GeV.

When the three considerations enumerated above are combined with the magnetic deflections predicted by (1) we arrive at the *cepa stratis* structure:

- in the energy range  $10^{10} \lesssim E/\text{GeV} \lesssim 10^{11}$  light (e.g.,  ${}^4\text{He}$ ,  ${}^{12}\text{C}$ ,  ${}^{14}\text{N}$ ,  ${}^{16}\text{O}$ ) nuclei are expected to survive the trip from nearby (distance  $\lesssim 50$  Mpc) sources, and these nuclei would suffer average deflections on the Galactic magnetic field of  $\theta \lesssim 15^\circ$ ;
- at the high energy ( $E \gtrsim 10^{11}$  GeV) end of the spectrum contributions come dominantly from heavier nuclei (e.g.,  ${}^{28}\text{Si}$ ,  ${}^{56}\text{Fe}$ ), leading to larger deflection angles associated to a decrease in rigidity.

To get a rough estimate of the maximum energy observed on Earth we translate the mfp shown in Fig. 4 into a cutoff energy in the spectrum for the various species as a function of the source distance  $D$ . The results are listed in Table II.

#### IV. DEFLECTIONS ON MAGNETIC FIELDS

Our understanding of the extragalactic magnetic field strength is surprisingly vague. Measurements of diffuse radio emission from the bridge area between the Coma and Abell superclusters [69] provide an estimate of  $\mathcal{O}(0.2 - 0.6) \mu\text{G}$  for the magnetic field in this region, assuming the contributions of the magnetic field and the relativistic particles are approximately equal (equipartition condition). Fields of  $\mathcal{O}(\mu\text{G})$  have also been estimated in a more extensive study of 16 low redshift clusters [70]. It is usually conjectured that the observed  $B$ -fields result

from the amplification of much weaker seed fields. However, a concrete unified model to explain the initial weak seed fields is yet to see the light of day. Generally speaking, the models for the seed fields can be divided into two broad classes: (i) *cosmological models*, in which the seed fields are produced in the early universe; (ii) *astrophysical models*, in which the seed fields are generated by motions of the plasma in (proto)galaxies. The galactic-scale superwinds generated by the starbursts provide a particular example of astrophysical models. Actually, if most galaxies lived through an active phase in their history, one expects the magnetized outflows from their jets to also efficiently pollute the extragalactic medium. It is reasonable to suspect that the  $B$ -fields originating in this way would be randomly oriented within cells of sizes below the mean separation between galaxies,  $\lambda_B \lesssim 1$  Mpc.

Thus far the extremely weak unamplified extragalactic magnetic fields have escaped detection. Measurements of the Faraday rotation in the linearly polarized radio emission from distant quasars [71, 72] and/or distortions of the spectrum and polarization properties in the CMB [73, 74] yield upper limits on the extragalactic magnetic field strength as a function of the reversal scale. It is noteworthy that Faraday rotation measurements (RM) sample extragalactic magnetic fields of any origin (out to quasar distances), while the CMB analyses set limits *only* on primordial magnetic fields. The RM bounds are strongly dependent on assumptions about the electron density profile as a function of the redshift. If electron densities follow that of the Lyman- $\alpha$  forest [75], the average magnitude of the magnetic field receives an upper limit of  $B \sim 0.65$  nG for reversals on the scale of the horizon, and  $B \sim 1.7$  nG for reversal scales on the order of 1 Mpc, at the  $2\sigma$  level [76]. These upper limits are estimated assuming standard cosmological parameters [77].

In the limit of small deflections (expected for nG field strength) the typical deflection of UHECRs in the extragalactic magnetic field can be estimated to be

$$\theta \approx 0.15^\circ Z \sqrt{\frac{D}{3.8 \text{ Mpc}} \frac{\lambda_B}{0.1 \text{ Mpc}}} \left(\frac{B}{\text{nG}}\right) \left(\frac{10^{11} \text{ GeV}}{E}\right), \quad (8)$$

where  $D$  is the source distance and  $Z$  is the charge of the UHECR in units of the proton charge [78, 79]. It is then reasonably to assume that extragalactic deflections would generally be much smaller than those arising from the galactic magnetic field (GMF).

We now turn to study the effect of GMF on the deflection of UHECRs nuclei from the direction of nearby starburst and radio galaxies. We take the Jansson and Farrar (JF) model as a semi-realistic magnetic field model to investigate deflections as UHECRs travel through the Galaxy [8–10]. In the JF model the GMF is described by a superposition of three divergence-free large-scale regular components: a spiral disk field, a toroidal halo field, and a poloidal field. In addition, there is a turbu-

lent random magnetic field that follows a Kolmogorov distribution.

All the magnetic fields are implemented in the Runge-Kutta cosmic ray propagation simulation tool *CRT* [80]. The random magnetic field is produced within a cubic box of side 5.12 kpc. Inside this box, a different value of the magnetic field is produced in each of  $512^3$  equally spaced points. This box is then replicated and placed through the galactic space with different orientations, to cover the whole galaxy. For the random magnetic field, which is described as a superposition of waves of different wavelengths, we restrict them to range from 5 pc to 30 pc.

The parameters of the regular and random magnetic field are constrained by: (i) multi-frequency radio observations of the Faraday RM of extragalactic radio sources; (ii) measurements of the polarized synchrotron emission of cosmic ray electrons in the regular magnetic field of the Galaxy; (iii) measurements of the total (polarized and unpolarized) synchrotron intensity, which is a line-of-sight integral depending on the product of cosmic ray electron density and total transverse magnetic field strength (coherent and random).

Beginning with an isotropic distribution of arrival directions observed on Earth we back-propagate  $10^6$  nuclei to the border of the Galaxy for each of the species  $^4\text{He}$ ,  $^{14}\text{N}$ ,  $^{28}\text{Si}$ , and  $^{56}\text{Fe}$ . Although we have shown in Table I that in the energy range of interest the source spectra are rather soft, to illustrate the competition between energy loss during propagation and deflection on the GMF in a simple way we adopt hard energy spectra  $\propto E^{-1.5}$ , with a maximum energy  $E_{\text{max}} = 10^{11.5}$  GeV. We tally the fraction of events consistent with the directions in the sky of nearby starburst and radio galaxies. A summary of the corresponding deflections exhibited as Mollweide projections is shown in Figs. 5, 6 and 7. In Figs. 6 and 7 we have imposed the energy cuts for the different species given in Table II to account for the energy loss before reaching the Galaxy. One can draw the following conclusions:

- Our results are consistent with similar analyses using the same JF model and the hypotheses that M87 and Fornax A [81], or Cen A and M82 [12] are potential sources of UHECRs.
- We observe that the effect of the GMF is to modify the onion-like structure one would expect if there were purely random magnetic fields into more complex elongated banana shapes.
- A comparison of Fig. 5 with the observed excess map of Fig. 2 indicates qualitative agreement with Auger data.
- It was proposed that Fornax A could explain the bulk of the Auger warm spot right of the Galactic south pole [45]. However, as shown in Fig. 7, the JF model predicts deflections which do not favor this association.

- A comparison of Figs. 2 and 6 shows that the JF model with selected turbulent parameters cannot explain the TA hot spot. However, the GMF in this region is dominated by turbulence (see e.g., Fig. 11 in [12]), which can accommodate an abundance of possible sky patterns that could be consistent with TA observations.

In the remainder of the paper we develop a test which a future mission such as POEMMA could use to clarify the nuclear composition of a given hot spot.

## V. TEST STATISTICS

We have seen that UHECRs coming from a given source in the sky are scattered around the line of sight to that source. Their arrival directions depend on the properties of the cosmic ray, as well as on the intergalactic and galactic media. Although the GMF is highly anisotropic, we will assume that the deflection of particles is isotropic around the line of sight. In general, one must consider the variations of the magnetic field for UHECRs arriving from different points of the sky. The anisotropies are rather large, as shown in Sec. IV. A full consideration of the anisotropic magnetic deflections would modify the distribution (10) below to include an azimuthal variable around the line of sight, and should also take into account its direction in the sky. Nevertheless, the procedure of the analysis would not change significantly. The assumption of isotropy around the line of sight allows us to demonstrate the search technique while keeping the complexity at a reasonable level at this stage.

Hereafter we assume that the magnitude of the deflection of a cosmic ray, with energy  $E$  and charge  $Ze$ , about the line of sight is given by (1). With this simplified picture of the effect that magnetic fields have on UHECRs, one can assume that cosmic rays are *normally* distributed around the source direction, which defines the center of the hot spot. The generalization of a normal distribution to directional data is the wrapped normal distribution, which can be approximated by the von Mises distribution [1]. In what follows we consider that the deflection  $\delta$ , which characterizes the angle between the arrival direction and the line of sight, to be a random variable distributed according to a one sided von Mises distribution, bounded by a window size  $\Delta$  with zero mean and a dispersion parameter  $\kappa = 1/\theta^2(E, Z)$ . Thus, its probability density function is

$$f_{\text{vM}}(\delta|E, Z) \propto \exp\left[\frac{\cos \delta}{\theta^2(E, Z)}\right] \Theta(\Delta - \delta). \quad (9)$$

The observed UHECR spectrum can be described as being proportional to  $\sum_A \sum_s w_{A,s} E^{-\gamma} \exp[-E/E_{A,s}(D)]$ , where  $E_{A,s}(D)$  is the cutoff energy that depends on the baryon number of the nucleus and the distance to its source; see Table II. Here, the weights  $w_{A,s}$  account for the various contributions of different species  $A$  for



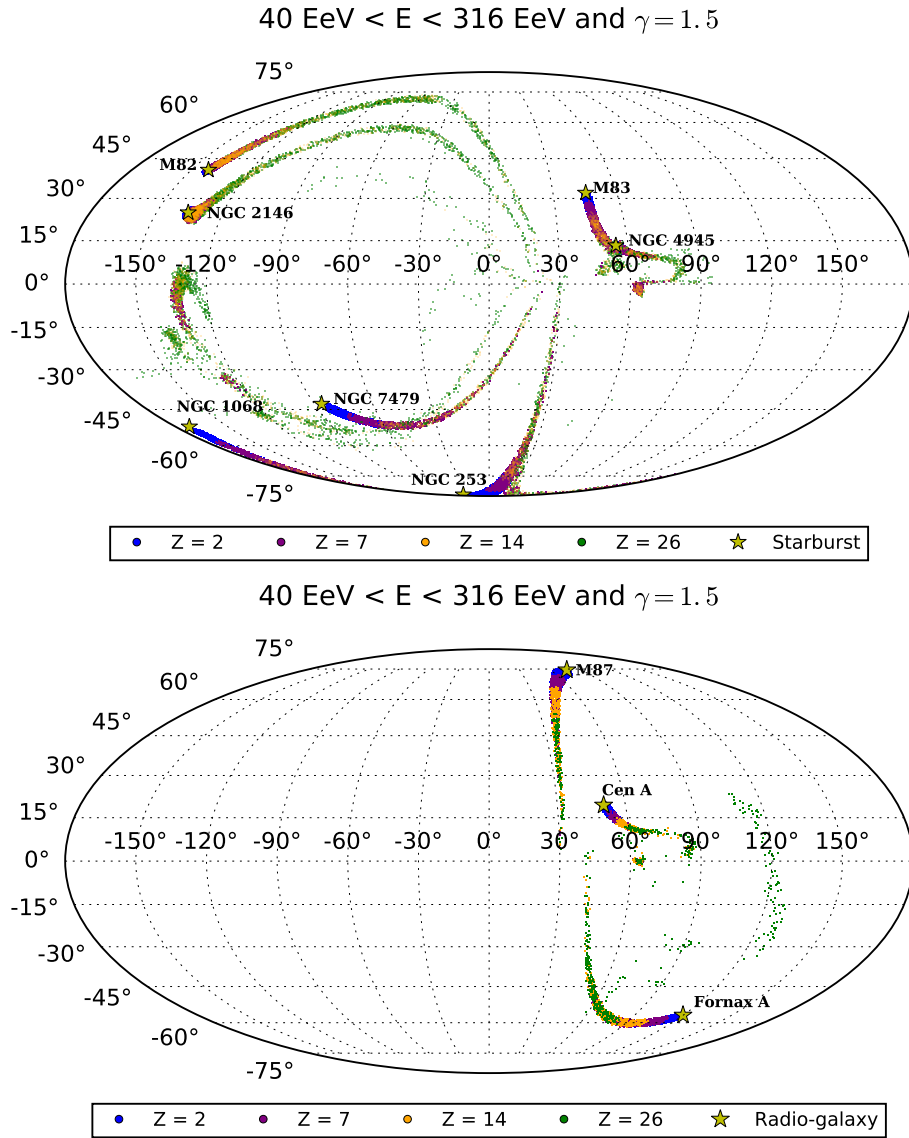


FIG. 5: Skymaps in Mollweide projection of the distribution of arrival directions for selected SGBs (up) and radiogalaxies (down). The sky maps are in Galactic coordinates.

a given source  $s$ . Moreover, a lower cut in the energies of interest is considered. Therefore, the probability density for a cosmic ray assumed to come from a distant point

source to have energy in  $[E, E + dE]$  and deflection in  $[\delta, \delta + d\delta]$  is

$$f(E, \delta | A, Z, z, \Delta, E_0) = \mathcal{A} E^{-\gamma} \exp\left[-\frac{E}{E_A(z)}\right] \exp\left[\frac{\cos \delta}{\theta^2(E, Z)}\right] \Theta(\Delta - \delta) \Theta(E - E_0), \quad (10)$$

where  $\mathcal{A}$  is a normalization constant. Since this distribution represents the measured spectrum, and not the actual spectrum at Earth, it must be understood that this probability density represents the distribution of the

events the experiment would record. If one wants to model the actual spectrum following (10), it would be necessary to add an energy dependent function modeling the response of the detector at different energies. In

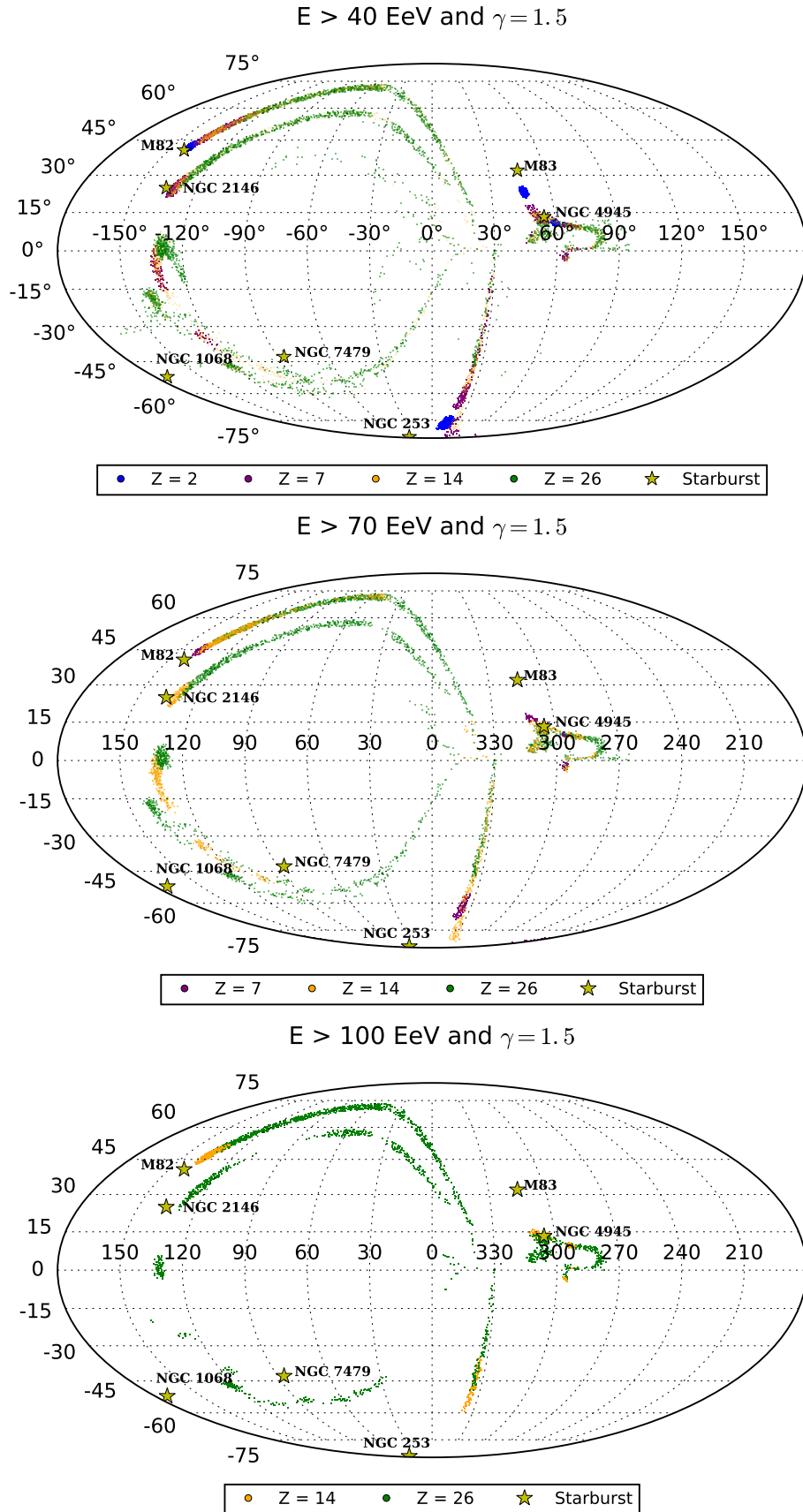


FIG. 6: Skymaps in Mollweide projection of the distribution of arrival directions for selected starbursts shown in Fig. 4 here indicated with yellow star. In all the cases we adopted a hard injection spectrum  $\propto E^{-1.5}$ , setting a threshold for the minimum energy of  $E_{\min}/\text{EeV} = 40, 70, 100$  from top to bottom. We have also imposed the cuts given in Table II. The sky maps are in Galactic coordinates.

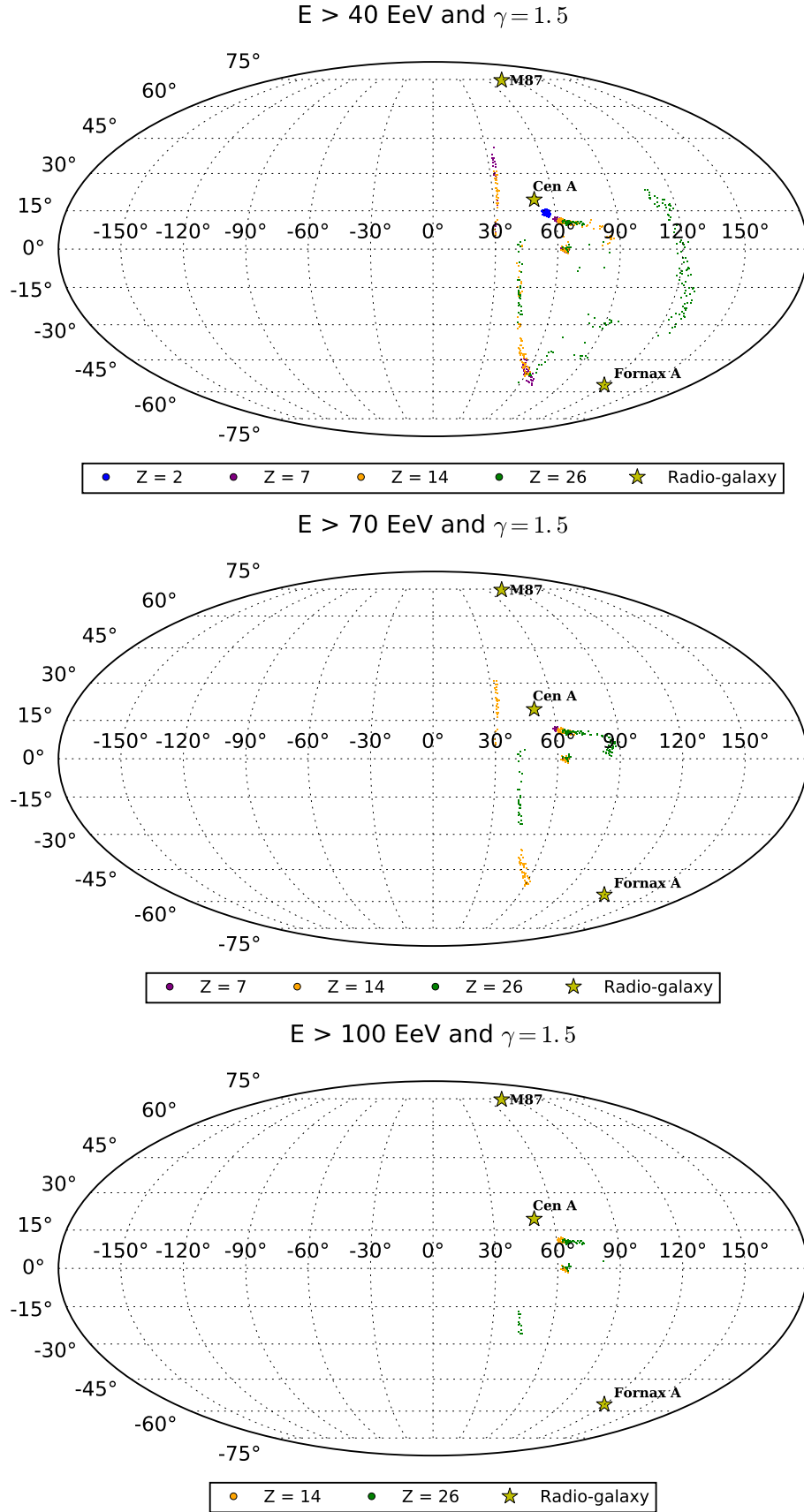


FIG. 7: Skymaps in Mollweide projection of the distribution of arrival directions for selected radio galaxies also shown in Fig. 4 here indicated with a yellow star. In all the cases we adopted a hard injection spectrum  $\propto E^{-1.5}$ , setting a threshold for the minimum energy of  $E_{\min}/\text{EeV} = 40, 70, 100$  from top to bottom. We have also imposed the cuts given in Table II. The sky maps are in Galactic coordinates.

a full study, this could be easily implemented without changing the techniques described below.

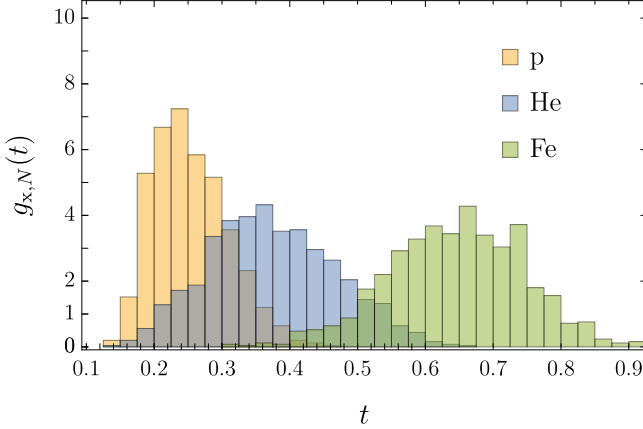


FIG. 8: PDF histograms for the test statistic empirical distribution for the null hypothesis (proton), helium and iron, with  $N = 20$ .

Once experimental data is collected, and a series of events within an angular window are selected to belong to some cosmic ray source, one can study their energies and deflections to extract, by means of (10), information about the composition of the source. Given the theoretical distributions presented above for different atomic numbers, statistical testing of the data will provide this information.

To carry out the statistical analysis we must first define the window size  $\Delta$  and the threshold energy  $E_0$ . Next, the source must be identified, *i.e.* we select  $D$ . After that we can calculate the likelihood that different probability distributions (for different nuclei) describe the data. This would allow an estimation of the nucleus producing the major contribution to a given hot spot. Furthermore, one could use the likelihood ratio for different nuclei as a tool to study our ability to distinguish them. In general terms, it is possible to propose a null hypothesis (*e.g.*, that the composition is only protons), simulate data following the null hypothesis ( $\mathcal{H}_0$ ) and, choosing a convenient test statistic, study its distribution for the generated data. Once real data are available, the value of the test statistic for that data will provide a way to test the null hypothesis.

The Kolmogorov-Smirnov (KS) test provides a computationally less expensive test statistic than the one coming from likelihood minimization. It allows for the comparison of empirical multivariate distributions to statistical models, and provides a method for judging to which extent some data is likely to follow a given statistical distribution. Given a set  $\mathcal{D}$  of (empirical or simulated) data points, it is possible to construct an empirical cumulative distribution function (CDF)  $\tilde{F}(E, \delta)$ , which counts the fraction of data points with energy below  $E$  and de-

flection below  $\delta$ .<sup>2</sup> The CDF for the null hypothesis is

$$F(E, \delta | \mathcal{H}_0) = \int_{E_0}^E dE' \int_0^\delta d\delta' f(E', \delta' | \mathcal{H}_0). \quad (11)$$

The KS test statistic for  $\mathcal{D}$  is

$$t = \sup_{E, \delta} |F(E, \delta | \mathcal{H}_0) - \tilde{F}(E, \delta)|, \quad (12)$$

where  $E \in [E_0, \infty]$  and  $\delta \in [0, \Delta]$ . If each dataset is simulated several times following the same statistical distribution, one can obtain not only a single value for  $t$ , but a distribution  $g(t)$  for its value. These distributions coming from different datasets will give information on the ability of the experiment and the test to probe a hypothesis.

The power of a statistical test is the probability that the null hypothesis is rejected if it is actually false. It is dependent on the significance level of the test  $\alpha$ , the probability of rejecting the null hypothesis while it is true. For a chosen null hypothesis  $\mathcal{H}_0$  and significance level  $\alpha$ , there is a critical value for the test statistic,  $t_c$ , above which there is a fraction  $\alpha$  of the data simulated following  $\mathcal{H}_0$ . For a given alternative hypothesis  $\mathcal{H}_k$ , the fraction  $\beta_k$  of the data with test statistic  $t < t_c$  is the probability of not rejecting the null hypothesis while it is false. Thus, the power of the test for a given alternative hypothesis is given by

$$\mathcal{P}_k = 1 - \beta_k = 1 - \int_0^{t_c} g_k(t) dt. \quad (13)$$

To exemplify this method, we simulate datasets  $\mathcal{D}_{x,N}$  following the distributions in (10), where  $x \in \{p, {}^4\text{He}, {}^{14}\text{N}, {}^{56}\text{Fe}\}$  and  $N = \dim \mathcal{D}_{x,N}$  is the number of data points in the hot spot. We assume (i) an angular window of  $\Delta = 13^\circ$ , (ii) a distance to the source of about 4 Mpc, similar to that of many of the sources considered above, (iii) an energy threshold at  $E_0 = 40 \text{ EeV}$ , (iv) and an exponent  $\gamma = 5.03$ , consistent with both the energy spectrum above 40 EeV reported by the Auger Collaboration [24] and the source spectra given in Table I. For each value of  $N$ , which roughly corresponds to a given life time of the experiment, we consider as null hypothesis a pure proton composition,  $\mathcal{H}_{p,N}$ , and the different nuclei as alternative hypotheses  $\mathcal{H}_{x,N}$ .

Each dataset is simulated  $10^3$  times to obtain the test statistic distributions. Some of them are shown in Fig. 8. The ability to distinguish the null from the alternative hypotheses decreases with the overlap of the different distributions. In Fig. 9 we show the

<sup>2</sup> More generally, one could consider CDFs defined as the fraction of events above  $E$  and  $\delta$ , or combinations of *above* and *below* for both variables. We do not study those cases here, without denying their relevance.

CDF  $G_{x,N}(t) = \int_0^t g_{x,N}(t') dt'$  for protons to illustrate how the choice of  $\alpha$  provides the critical values of  $t$  as  $G_{p,N}(t_{c,N}) = 1 - \alpha$ . Introducing the CDF in (13), the power is given as  $\mathcal{P}_{x,N} = 1 - G_{x,N}(t_{c,N})$ .

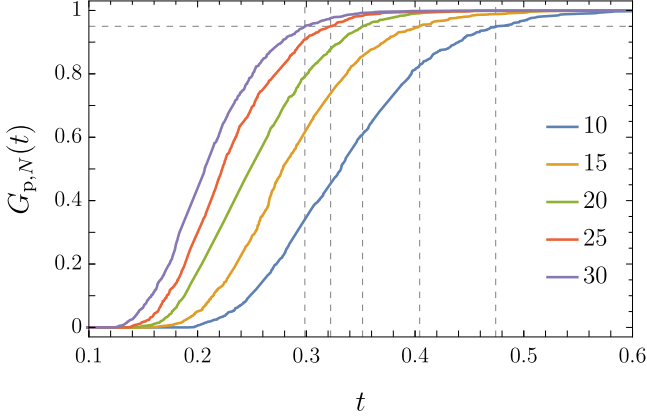


FIG. 9: CDF for the test statistic distribution for null hypotheses for various  $N$ . The dashed lines indicate the choice  $\alpha = 0.05$  and the corresponding critical values of the test statistic.

In Fig. 10 we show the statistical power of the test considering different alternative hypotheses, as a function of  $N$ . If the hot spot is composed of nuclei heavier than nitrogen, observation of  $N \gtrsim 20$  events will be required to discard a pure-proton explanation at the 95% CL.

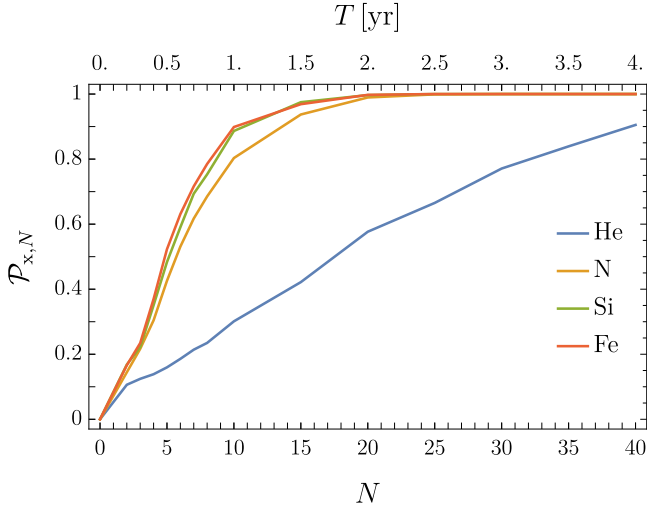


FIG. 10: Power of the statistical test for different alternative hypotheses, *i.e.* different nuclei and number of events per hot spot. The horizontal axis on the top indicates the projected time-scale for POEMMA.

The variation of the statistical power with the radius of the angular window is presented in Fig. 11 for the case of nitrogen, keeping constant the number of events per steradian.

We have briefly study the effects of considering a harder spectrum. This increases the number of high

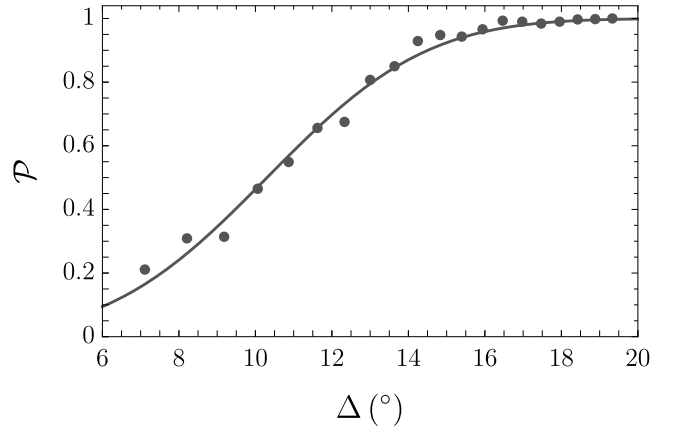


FIG. 11: Power of the statistical test for a nitrogen alternative hypothesis as a function of the angular radius of the window around the source. The number of events in the sky is fixed to have an expected number of 10 events in a  $13^\circ$  radius window. The curve shows a fit to the data with an error function.

energy nuclei, making the distributions of energy and arrival direction resemble more those of protons. Overall, the test statistic distributions for nuclei shift to lower values, increasing the overlap with the proton distributions. In Fig. 12 we show the comparison between the statistical power for soft and hard spectra for nitrogen.

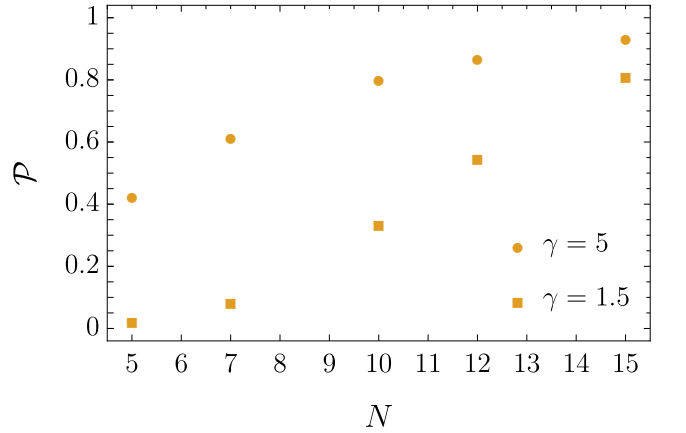


FIG. 12: Power of the statistical test for a nitrogen alternative hypothesis for a hard ( $\gamma = 1.5$ ) and a soft ( $\gamma = 5$ ) spectrum, as a function of the number of events in the hotspot. All the other parameters are unaltered with respect to those in Fig. 10.

It should be clarified that this method is not meant to obtain the most probable composition of the source, nor to obtain the contributions of different nuclei to a given hotspot. We illustrate a method to reject a pure composition scenario. In order to obtain a more detailed information about the composition of the hotspot, it would be possible to add several terms like (10) with different weights for different nuclei, and estimate the values of the weights from the data. Nevertheless, it can be safely



stated that the power to distinguish a mixed composition sample from a pure proton composition with this method will never be lower than that to distinguish the lightest nuclei in the sample from protons. In any other situation (trying to reject a nuclei pure composition or a mixed composition), the power will decrease with respect to that presented here, as the overlap between the test statistic distributions will increase.

## VI. POEMMA SENSITIVITY

The NASA's POEMMA mission design [17] combines the concept developed for the Orbiting Wide-field Light-collectors (OWL) [82] mission and the recently proposed Cherenkov from Astrophysical Neutrinos Telescope (CHANT) [83] concept to form a multi-messenger probe of the most extreme environments in the Universe. Building on the OWL concept, POEMMA is composed of two identical satellites flying in formation with the ability to observe overlapping regions during moonless nights at angles ranging from nadir to just above the limb of the Earth. For a rough estimate of the expected event rate, we consider the orbit of POEMMA at an altitude 525 km with a separation between satellites of 300 km each with a field of view of  $45^\circ$ . The area observed in stereo at nadir is approximately  $1.46 \times 10^5 \text{ km}^2$ , yielding an instantaneous aperture  $\sim 4.6 \times 10^5 \text{ km}^2 \text{ sr}$ . Preliminary studies on trigger efficiency and the optical performance of POEMMA indicate the detector will be fully efficient above about  $10^{11} \text{ GeV}$ . We define the acceptance conditions such that the background from airglow in the entire focal plane produces a rate below 1 kHz. We require signal above threshold in both satellites. Herein we estimate the expected number of events by scaling the number observed at Auger according to the ratio of the POEMMA to Auger exposures. More precisely, in Fig. 13 we compare the exposure to be collected in 5 yr by POEMMA, assuming a conservative 10% duty cycle, with the exposure collected by the Auger surface array as reported in [24]. The ratio of the exposures is roughly an order of magnitude larger when comparing with the data collected by the fluorescence detectors of Auger. The ratio of the number of events (POEMMA vs Auger, bin by bin of energy) is readable from the exposure scaling.

In order to make estimations about the future performance of POEMMA for the task presented in Sec. V, we present an estimation of the typical sample size of a  $13^\circ$  hot spot as a function of time. The estimate shown in Fig. 13 gives an event rate of  $\Gamma \sim 250 \text{ yr}^{-1}$ . A  $13^\circ$  angular radius solid angle covers a fraction  $f_{\text{sky}} \sim 0.013$  of the sky. Within a hot spot, one expects both background and source contributions, with a ratio  $f_{\text{events}} = n_{\text{ev}}/n_{\text{bg}}$ . With this, the required life time of the experiment to measure

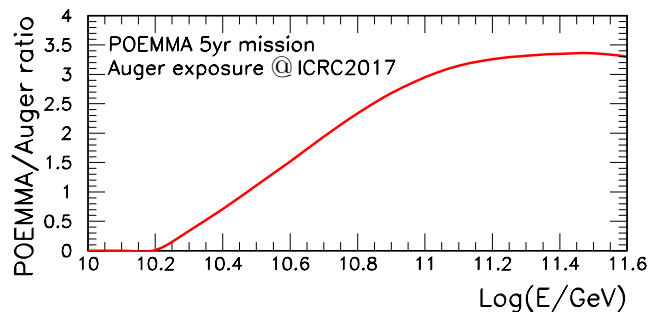


FIG. 13: Ratio of the expected exposure of POEMMA after 5 yr of operation and the exposure collected by the surface array of the Pierre Auger Observatory as reported at the 35th International Cosmic Ray Conference (ICRC 2017) [24].

a hot spot of  $N$  events can be roughly estimated to be

$$T \sim \frac{N}{\Gamma f_{\text{sky}} f_{\text{events}}}. \quad (14)$$

For  $f_{\text{events}} \sim 3$ , as observed in [24] from the direction of Cen A,  $T \sim 0.1N \text{ yr}$ .<sup>3</sup> The projected sensitivity of POEMMA is shown in Fig. 10. For hot spots of 20 or more events, the discovery power (with  $\alpha = 0.05$ ) is almost one for nuclei other than helium. Therefore, we conclude that if the hot spot is composed of nuclei heavier than nitrogen, in two years of operation POEMMA will be able to exclude a pure-proton origin at the 95% CL.

## VII. CONCLUSIONS

In the spirit of [16], we have developed a statistical test to quantify the ability of the future NASA's POEMMA mission to isolate the nuclear composition of UHECRs using a subsample of the distribution of arrival directions associated with a particular source  $\rightleftharpoons$  hot spot in the cosmic-ray-sky. This is possible because sources of UHECR protons exhibit anisotropy patterns which become denser and compressed with rising energy, whereas nucleus-emitting-sources give rise to a cepa stratis structure with layers that become more distant from the source position with rising energy. The peculiar shape of the hot spots from nucleus-accelerators is steered by the competition between energy loss during propagation and deflection on the GMF.

Our conclusions and caveats can be encapsulated as follows:

- We have shown that if an UHECR hot spot is composed of nuclei heavier than nitrogen, observation of roughly 20 events in this region of the sky will

<sup>3</sup> We are not claiming that this is the value to expect, but just showing a possible value.

be required to discard a pure-proton explanation at the 95% CL.

- We have used the excess of events reported by the Auger Collaboration from the direction of Cen A [24] to project that about 2 yr of POEMMA running will be necessary to probe the nuclear composition of this hot spot.
- The magnetic field structure is not as simple as it has been considered here. It presents a highly anisotropic structure that would force us to consider its complexity in several ways: simulations should be performed individually for each source, propagating the cosmic rays from the source to Earth; and the distributions and data should include another angular variable to measure the orientation about the line of sight.
- The background should be considered in this picture. The presence of a background with or without a single nuclear composition would somewhat deteriorate our ability to reject a given hypothesis.
- We have considered as known, and equal, the power law for all the energy spectra. Variations from this behavior could also have an effect on our results.
- Both the angular and energy reconstruction resolution of POEMMA have to be considered in a complete analysis. The angular resolution, roughly estimated to be of the order of  $1^\circ$ , should not degrade the quality of our analysis significantly. The estimated 20% energy resolution is also expected to have a minor impact. Indeed the uncertainties introduced by these considerations would fall within errors of our working assumptions.

In summary, in a few years of operation the future NASA's POEMMA mission will provide an *a priori* test of the evidence for hot spots reported by the Auger [20, 24]

and TA [37] collaborations. We have shown that POEMMA satellite stereo observations will be able to determine the UHECR composition using the distribution of arrival directions. This new method to determine the nature of the particle species is *complementary* to those using observables of extensive air showers, and therefore is unaffected by the large systematic uncertainties of hadronic interaction models.

### Acknowledgments

We thank our colleagues of the Pierre Auger and POEMMA collaborations for some valuable discussions. The research of RCdA is supported by the Fulbright Scholarship Program (Junior Faculty Member Award) and CNPq under Grant 307750/2017-5. She also thanks the Physics and Astronomy Department at Lehman College for hospitality. The research of JFS and LAA is supported by the by the U.S. National Science Foundation (NSF Grant PHY-1620661) and the National Aeronautics and Space Administration (NASA Grant 80NSSC18K0464). TCP has also been partially supported by NASA Grant 80NSSC18K0464. The research of DFT is supported by grants AYA2015-71042-P, AYA2017-92402-EXP, iLink 2017-1238, and SGR 2017-1383. TADP and RJM were supported in part by NSF grant AST-1153335. The research of FS and LW is supported by NASA APRA NNX13AH55G. The POEMMA concept study is funded by NASA Award NNX17AJ82 at the University of Chicago and Goddard Space Flight Center. We acknowledge the National Laboratory for Scientific Computing (LNCC/MCTI, Brazil) for providing HPC resources of the SDumont supercomputer, which have contributed to the research results reported within this paper. URL: <http://sdumont.lncc.br>. Any opinions, findings, and conclusions or recommendations expressed in this material are those of the authors and do not necessarily reflect the views of the NSF or NASA.

- 
- [1] L. A. Anchordoqui, *Ultra-high-energy cosmic rays*, arXiv:1807.09645 [astro-ph.HE].
- [2] K. Kotera and A. V. Olinto, *The astrophysics of ultra-high energy cosmic rays*, *Ann. Rev. Astron. Astrophys.* **49**, 119 (2011) doi:10.1146/annurev-astro-081710-102620 [arXiv:1101.4256 [astro-ph.HE]].
- [3] A. Aab *et al.* [Pierre Auger Collaboration], *Depth of maximum of air-shower profiles at the Pierre Auger Observatory I: Measurements at energies above  $10^{17.8}$  eV*, *Phys. Rev. D* **90**, no. 12, 122005 (2014) doi:10.1103/PhysRevD.90.122005 [arXiv:1409.4809 [astro-ph.HE]].
- [4] A. Aab *et al.* [Pierre Auger Collaboration], *Depth of maximum of air-shower profiles at the Pierre Auger Observatory II: Composition implications*, *Phys. Rev. D* **90**, no. 12, 122006 (2014) doi:10.1103/PhysRevD.90.122006 [arXiv:1409.5083 [astro-ph.HE]].
- [5] A. Aab *et al.* [Pierre Auger Collaboration], *Evidence for a mixed mass composition at the “ankle” in the cosmic-ray spectrum*, *Phys. Lett. B* **762**, 288 (2016) doi:10.1016/j.physletb.2016.09.039 [arXiv:1609.08567 [astro-ph.HE]].
- [6] R. Abbasi *et al.* [Pierre Auger and Telescope Array Collaborations], *Report of the working group on the composition of ultrahigh energy cosmic rays*, arXiv:1503.07540 [astro-ph.HE].
- [7] M. S. Pshirkov, P. G. Tinyakov, P. P. Kronberg and K. J. Newton-McGee, *Deriving global structure of the Galactic magnetic field from Faraday rotation measures of extragalactic sources*, *Astrophys. J.* **738**, 192 (2011) doi:10.1088/0004-637X/738/2/192 [arXiv:1103.0814 [astro-ph.GA]].

- [8] R. Jansson and G. R. Farrar, **A new model of the Galactic magnetic field**, *Astrophys. J.* **757**, 14 (2012) doi:10.1088/0004-637X/757/1/14 [arXiv:1204.3662 [astro-ph.GA]].
- [9] R. Jansson and G. R. Farrar, **The Galactic magnetic field**, *Astrophys. J.* **761**, L11 (2012) doi:10.1088/2041-8205/761/1/L11 [arXiv:1210.7820 [astro-ph.GA]].
- [10] M. Unger and G. R. Farrar, **Uncertainties in the magnetic field of the Milky Way**, *PoS ICRC 2017*, 558 (2017) [arXiv:1707.02339 [astro-ph.GA]].
- [11] M. Erdmann, G. Müller, M. Urban and M. Wirtz, **The nuclear window to the extragalactic universe**, *Astropart. Phys.* **85**, 54 (2016) doi:10.1016/j.astropartphys.2016.10.002 [arXiv:1607.01645 [astro-ph.HE]].
- [12] G. R. Farrar and M. S. Sutherland, **Deflections of UHECRs in the Galactic magnetic field**, arXiv:1711.02730 [astro-ph.HE].
- [13] K. Greisen, **End to the cosmic ray spectrum?**, *Phys. Rev. Lett.* **16**, 748 (1966) doi:10.1103/PhysRevLett.16.748.
- [14] G. T. Zatsepin and V. A. Kuzmin, **Upper limit of the spectrum of cosmic rays**, *JETP Lett.* **4**, 78 (1966) [*Pisma Zh. Eksp. Teor. Fiz.* **4**, 114 (1966)].
- [15] J. L. Puget, F. W. Stecker and J. H. Bredekamp, **Photonuclear interactions of ultrahigh-energy cosmic rays and their astrophysical consequences**, *Astrophys. J.* **205**, 638 (1976). doi:10.1086/154321
- [16] L. A. Anchordoqui, V. Barger and T. J. Weiler, **Cosmic mass spectrometer**, *JHEAp* **17**, 38 (2018) doi:10.1016/j.jheap.2017.12.001 [arXiv:1707.05408 [astro-ph.HE]].
- [17] A. V. Olinto *et al.*, **POEMMA: Probe Of Extreme Multi-Messenger Astrophysics**, *PoS ICRC 2017*, 542 (2018) doi:10.22323/1.301.0542 [arXiv:1708.07599 [astro-ph.IM]].
- [18] J. Biteau *et al.* [Telescope Array and Pierre Auger Collaborations], **Covering the sphere at ultra-high energies: full-sky cosmic-ray maps beyond the ankle and the flux suppression**, To be published in Proceedings of Ultra High Energy Cosmic Rays 2018, 8 - 12 October 2018, Paris.
- [19] L. A. Anchordoqui, H. Goldberg and D. F. Torres, **Anisotropy at the end of the cosmic ray spectrum?**, *Phys. Rev. D* **67**, 123006 (2003) doi:10.1103/PhysRevD.67.123006 [astro-ph/0209546].
- [20] A. Aab *et al.* [Pierre Auger Collaboration], **Indication of anisotropy in arrival directions of ultrahigh-energy cosmic rays through comparison to the flux pattern of extragalactic gamma-ray sources**, *Astrophys. J.* **853**, no. 2, L29 (2018) doi:10.3847/2041-8213/aaa66d [arXiv:1801.06160 [astro-ph.HE]].
- [21] M. Ackermann *et al.* [Fermi-LAT Collaboration], **GeV observations of star-forming galaxies with Fermi-LAT**, *Astrophys. J.* **755**, 164 (2012) doi:10.1088/0004-637X/755/2/164 [arXiv:1206.1346 [astro-ph.HE]].
- [22] J. Abraham *et al.* [Pierre Auger Collaboration], **Observation of the suppression of the flux of cosmic rays above  $4 \times 10^{19}$  eV**, *Phys. Rev. Lett.* **101**, 061101 (2008) doi:10.1103/PhysRevLett.101.061101 [arXiv:0806.4302 [astro-ph]].
- [23] J. Abraham *et al.* [Pierre Auger Collaboration], **Measurement of the energy spectrum of cosmic rays above  $10^{18}$  eV using the Pierre Auger Observatory**, *Phys. Lett. B* **685**, 239 (2010) doi:10.1016/j.physletb.2010.02.013 [arXiv:1002.1975 [astro-ph.HE]].
- [24] A. Aab *et al.* [Pierre Auger Collaboration], **The Pierre Auger Observatory: Contributions to the 35th International Cosmic Ray Conference (ICRC 2017)**, arXiv:1708.06592 [astro-ph.HE].
- [25] M. Ackermann *et al.* [Fermi-LAT Collaboration], **2FHL: The second catalog of hard Fermi-LAT sources**, *Astrophys. J. Suppl.* **222**, no. 1, 5 (2016) doi:10.3847/0067-0049/222/1/5 [arXiv:1508.04449 [astro-ph.HE]].
- [26] R. U. Abbasi *et al.* [Telescope Array Collaboration], **Indications of intermediate-scale anisotropy of cosmic rays with energy greater than 57 EeV in the Northern sky measured with the surface detector of the Telescope Array experiment**, *Astrophys. J.* **790**, L21 (2014) doi:10.1088/2041-8205/790/2/L21 [arXiv:1404.5890 [astro-ph.HE]].
- [27] K. Kawata *et al.* [Telescope Array Collaboration], **Ultra-high-energy cosmic-ray hotspot observed with the Telescope Array surface detectors**, *PoS ICRC 2015*, 276 (2016). doi:10.7566/JPSCP.19.011020
- [28] A. di Matteo *et al.*, **Arrival directions of cosmic rays at ultra-high energies**, *JPS Conf. Proc.* **19**, 011020 (2018). doi:10.7566/JPSCP.19.011020
- [29] T.-P. Li and Y.-Q. Ma, **Analysis methods for results in gamma-ray astronomy**, *Astrophys. J.* **272**, 317 (1983). doi:10.1086/161295
- [30] The RGB color components of the skymap and legend presented in [18] were sampled taking enough points per pixel to ensure that no information is lost. To each point sampled from the skymap, we associate a value for the Li-Ma significance given by the corresponding value of the legend pixel that is closest to the skymap pixel. The closeness is measured by a euclidean distance in the RGB space. The coordinates of the pixels were transformed successively by an inverse Mollweide projection, an equatorial to galactic coordinate transformation, and a Mollweide projection to create the new skymap shown in this figure.
- [31] L. A. Anchordoqui, T. C. Paul, L. H. M. da Silva, D. F. Torres and B. J. Vlcek, **What IceCube data tell us about neutrino emission from star-forming galaxies (so far)**, *Phys. Rev. D* **89**, no. 12, 127304 (2014) doi:10.1103/PhysRevD.89.127304 [arXiv:1405.7648 [astro-ph.HE]].
- [32] K. Fang, T. Fujii, T. Linden and A. V. Olinto, **Is the ultra-high energy cosmic-ray excess observed by the Telescope Array correlated with IceCube neutrinos?**, *Astrophys. J.* **794**, no. 2, 126 (2014) doi:10.1088/0004-637X/794/2/126 [arXiv:1404.6237 [astro-ph.HE]].
- [33] H. N. He, A. Kusenko, S. Nagataki, B. B. Zhang, R. Z. Yang and Y. Z. Fan, **Monte Carlo Bayesian search for the plausible source of the Telescope Array hot spot**, *Phys. Rev. D* **93**, 043011 (2016) doi:10.1103/PhysRevD.93.043011 [arXiv:1411.5273 [astro-ph.HE]].
- [34] D. N. Pfeffer, E. D. Kovetz and M. Kamionkowski, **Ultrahigh-energy cosmic ray hotspots from tidal disruption events**, *Mon. Not. Roy. Astron. Soc.* **466**, no. 3, 2922 (2017) doi:10.1093/mnras/stw3337 [arXiv:1512.04959 [astro-ph.HE]].
- [35] R. Attallah and D. Bouchachi, **Ultrahigh energy cosmic rays from nearby starburst galaxies**, doi:10.1093/mnras/sty986 arXiv:1804.06603 [astro-ph.HE].
- [36] R. U. Abbasi *et al.* [Telescope Array Collaboration], **Search for correlations between arrival directions of ultrahigh-energy cosmic rays detected by the Telescope Array experiment and a flux pattern from nearby starburst galaxies**, [arXiv:1809.01573 [astro-ph.HE]].
- [37] R. U. Abbasi *et al.* [HiRes Collaboration], **First observation of the Greisen-Zatsepin-Kuzmin suppression**, *Phys. Rev. Lett.* **100**, 101101 (2008) doi:10.1103/PhysRevLett.100.101101 [astro-ph/0703099].



- [38] T. Abu-Zayyad *et al.* [Telescope Array Collaboration], **The cosmic ray energy spectrum observed with the surface detector of the Telescope Array experiment**, *Astrophys. J.* **768**, L1 (2013) doi:10.1088/2041-8205/768/1/L1 [arXiv:1205.5067 [astro-ph.HE]].
- [39] P. L. Biermann and P. A. Strittmatter, **Synchrotron emission from shock waves in active galactic nuclei**, *Astrophys. J.* **322**, 643 (1987). doi:10.1086/165759
- [40] J. P. Rachen and P. L. Biermann, **Extragalactic ultrahigh-energy cosmic rays I: Contribution from hot spots in FR-II radio galaxies**, *Astron. Astrophys.* **272**, 161 (1993) [astro-ph/9301010].
- [41] L. A. Anchordoqui, G. E. Romero and J. A. Combi, **Heavy nuclei at the end of the cosmic ray spectrum?**, *Phys. Rev. D* **60**, 103001 (1999) doi:10.1103/PhysRevD.60.103001 [astro-ph/9903145].
- [42] P. Blasi, R. I. Epstein and A. V. Olinto, **Ultrahigh-energy cosmic rays from young neutron star winds**, *Astrophys. J.* **533**, L123 (2000) doi:10.1086/312626 [astro-ph/9912240].
- [43] J. Arons, **Magnetars in the metagalaxy: an origin for ultrahigh-energy cosmic rays in the nearby universe**, *Astrophys. J.* **589**, 871 (2003) doi:10.1086/374776 [astro-ph/0208444].
- [44] A. Aab *et al.* [Pierre Auger Collaboration], **Searches for anisotropies in the arrival directions of the highest energy cosmic rays detected by the Pierre Auger Observatory**, *Astrophys. J.* **804**, no. 1, 15 (2015) doi:10.1088/0004-637X/804/1/15 [arXiv:1411.6111 [astro-ph.HE]].
- [45] J. H. Matthews, A. R. Bell, K. M. Blundell and A. T. Araudo, **Fornax A, Centaurus A and other radio galaxies as sources of ultra-high energy cosmic rays**, doi:10.1093/mnras/sly099 arXiv:1805.01902 [astro-ph.HE].
- [46] E. Waxman, **Cosmological gamma-ray bursts and the highest energy cosmic rays**, *Phys. Rev. Lett.* **75**, 386 (1995) doi:10.1103/PhysRevLett.75.386 [astro-ph/9505082].
- [47] L. A. Anchordoqui, **Acceleration of ultrahigh-energy cosmic rays in starburst superwinds**, *Phys. Rev. D* **97**, no. 6, 063010 (2018) doi:10.1103/PhysRevD.97.063010 [arXiv:1801.07170 [astro-ph.HE]].
- [48] B. Adebahr, M. Krause, U. Klein, M. Wezgowiec, D. J. Bomans and R.-J. Dettmar, **M82 - A radio continuum and polarisation study I: Data reduction and cosmic ray propagation**, *Astron. Astrophys.* **555**, A23 (2013) doi:10.1051/0004-6361/201220226 [arXiv:1209.5552 [astro-ph.GA]].
- [49] B. Adebahr, M. Krause, U. Klein, G. Heald, and R.-J. Dettmar, **M82 - A radio continuum and polarisation study II: Polarization and rotation measures**, *Astron. Astrophys.* **608**, A29 (2017) doi:10.1051/0004-6361/201629616 [arXiv:1710.04050 [astro-ph.GA]].
- [50] R. Beck, C. L. Carilli, M. A. Holdaway, and U. Klein, **Multifrequency observations of the radio continuum emission from NGC 253 I: Magnetic fields and rotation measures in the bar and halo**, *Astron. Astrophys.* **292**, 409 (1994).
- [51] V. Heesen, R. Beck, M. Krause and R.-J. Dettmar, **Cosmic rays and the magnetic field in the nearby starburst galaxy NGC 253 I: The distribution and transport of cosmic rays**, *Astron. Astrophys.* **494**, 563 (2009) doi:10.1051/0004-6361:200810543 [arXiv:0812.0346 [astro-ph]].
- [52] V. Heesen, M. Krause, R. Beck and R. J. Dettmar, **Cosmic rays and the magnetic field in the nearby starburst galaxy NGC 253 II: The magnetic field structure**, *Astron. Astrophys.* **506**, 1123 (2009) doi:10.1051/0004-6361/200911698 [arXiv:0908.2985 [astro-ph.CO]].
- [53] V. Heesen, R. Beck, M. Krause and R. J. Dettmar, **Cosmic rays and the magnetic field in the nearby starburst galaxy NGC 253 III: Helical magnetic fields in the nuclear outflow**, *Astron. Astrophys.* **535**, A79 (2011) doi:10.1051/0004-6361/201117618 [arXiv:1109.0255 [astro-ph.CO]].
- [54] M. Krause, **Magnetic fields and halos in spiral galaxies**, arXiv:1401.1317 [astro-ph.GA].
- [55] T. A. Thompson, E. Quataert, E. Waxman, N. Murray and C. L. Martin, **Magnetic fields in starburst galaxies and the origin of the fir-radio correlation**, *Astrophys. J.* **645**, 186 (2006) [astro-ph/0601626].
- [56] B. C. Lacki and R. Beck, **The equipartition magnetic field formula in starburst galaxies: Accounting for pionic secondaries and strong energy losses**, *Mon. Not. Roy. Astron. Soc.* **430**, 3171 (2013) doi:10.1093/mnras/stt122 [arXiv:1301.5391 [astro-ph.CO]].
- [57] D. F. Torres, **Theoretical modelling of the diffuse emission of gamma-rays from extreme regions of star formation: The Case of Arp 220**, *Astrophys. J.* **617**, 966 (2004) doi:10.1086/425415 [astro-ph/0407240].
- [58] J. McBride, T. Robishaw, C. Heiles, G. C. Bower, and A. P. Sarma, **Parsec-scale magnetic fields in Arp 220**, *Mon. Not. Roy. Astron. Soc.* **447**, 1103 (2015) doi:10.1093/mnras/stu2489 [arXiv:1411.7407].
- [59] D. F. Torres, A. Cillis, B. Lacki and Y. Rephaeli, **Building up the spectrum of cosmic-rays in star-forming regions**, *Mon. Not. Roy. Astron. Soc.* **423**, 822 (2012) doi:10.1111/j.1365-2966.2012.20920.x [arXiv:1203.2798 [astro-ph.HE]].
- [60] T. A. D. Paglione and R. D. Abrahams, **Properties of nearby starburst galaxies based on their diffuse gamma-ray emission**, *Astrophys. J.* **755**, 106 (2012) doi:10.1088/0004-637X/755/2/106 [arXiv:1206.3530 [astro-ph.HE]].
- [61] E. Domingo-Santamaria and D. F. Torres, **High energy gamma-ray emission from the starburst nucleus of NGC 253**, *Astron. Astrophys.* **444**, 403 (2005) doi:10.1051/0004-6361:20053613 [astro-ph/0506240].
- [62] E. de Cea del Pozo, D. F. Torres and A. Y. R. Marrero, **Multi-messenger model for the starburst galaxy M82**, *Astrophys. J.* **698**, 1054 (2009) doi:10.1088/0004-637X/698/2/1054 [arXiv:0901.2688 [astro-ph.GA]].
- [63] B. C. Lacki, **Sturm und drang: Supernova-driven turbulence, magnetic fields, and cosmic rays in the chaotic starburst interstellar medium**, arXiv:1308.5232 [astro-ph.CO].
- [64] F. W. Stecker, **Photodisintegration of ultrahigh-energy cosmic rays by the universal radiation field**, *Phys. Rev.* **180**, 1264 (1969). doi:10.1103/PhysRev.180.1264
- [65] R. Alves Batista *et al.*, **CRPropa 3 - a Public Astrophysical Simulation Framework for Propagating Extragalactic Ultra-High Energy Particles**, *JCAP* **1605**, no. 05, 038 (2016) doi:10.1088/1475-7516/2016/05/038 [arXiv:1603.07142 [astro-ph.IM]].
- [66] J. F. Soriano, L. A. Anchordoqui and D. F. Torres, **Photo-disintegration of  $^4\text{He}$  on the cosmic microwave background is less severe than earlier thought**, *Phys. Rev. D* **98**, 043001 (2018) doi:10.1103/PhysRevD.98.043001 [arXiv:1805.00409 [astro-ph.HE]].
- [67] D. J. Fixsen, **The temperature of the cosmic microwave background**, *Astrophys. J.* **707**, 916 (2009) doi:10.1088/0004-637X/707/2/916 [arXiv:0911.1955 [astro-ph.CO]].
- [68] R. C. Gilmore, R. S. Somerville, J. R. Primack and A. Dominguez, **Semi-analytic modeling of the EBL and consequences for extragalactic gamma-ray spectra**, *Mon. Not. Roy. Astron. Soc.* **422**, 3189 (2012) doi:10.1111/j.1365-

- 2966.2012.20841.x [arXiv:1104.0671 [astro-ph.CO]].
- [69] K.-T. Kim, P. P. Kronberg, G. Giovannini and T. Venturi, **Discovery of intergalactic radio emission in the Coma-A1367 supercluster**, *Nature* **341**, 720 (1989) doi:10.1038/341720a0
- [70] T. E. Clarke, P. P. Kronberg and H. Boehringer, **A New radio – X-ray probe of galaxy cluster magnetic fields**, *Astrophys. J.* **547**, L111 (2001) doi:10.1086/318896 [astro-ph/0011281].
- [71] P. P. Kronberg, **Extragalactic magnetic fields**, *Rept. Prog. Phys.* **57**, 325 (1994). doi:10.1088/0034-4885/57/4/001
- [72] G. R. Farrar and T. Piran, **GZK violation: A Tempest in a (magnetic) teapot?**, *Phys. Rev. Lett.* **84**, 3527 (2000) doi:10.1103/PhysRevLett.84.3527 [astro-ph/9906431].
- [73] J. D. Barrow, P. G. Ferreira and J. Silk, **Constraints on a primordial magnetic field**, *Phys. Rev. Lett.* **78**, 3610 (1997) doi:10.1103/PhysRevLett.78.3610 [astro-ph/9701063].
- [74] K. Jedamzik, V. Katalinic and A. V. Olinto, **A limit on primordial small scale magnetic fields from CMB distortions**, *Phys. Rev. Lett.* **85**, 700 (2000) doi:10.1103/PhysRevLett.85.700 [astro-ph/9911100].
- [75] P. Blasi, S. Bures and A. V. Olinto, **Cosmological magnetic fields limits in an inhomogeneous universe**, *Astrophys. J.* **514**, L79 (1999) doi:10.1086/311958 [astro-ph/9812487].
- [76] M. S. Pshirkov, P. G. Tinyakov and F. R. Urban, **New limits on extragalactic magnetic fields from rotation measures**, *Phys. Rev. Lett.* **116**, no. 19, 191302 (2016) doi:10.1103/PhysRevLett.116.191302 [arXiv:1504.06546 [astro-ph.CO]].
- [77] M. Tanabashi *et al.* [Particle Data Group], **Review of Particle Physics**, *Phys. Rev. D* **98**, no. 3, 030001 (2018). doi:10.1103/PhysRevD.98.030001
- [78] E. Waxman and J. Miralda-Escude, **Images of bursting sources of high-energy cosmic rays I: Effects of magnetic fields**, *Astrophys. J.* **472**, L89 (1996) doi:10.1086/310367 [astro-ph/9607059].
- [79] G. R. Farrar, R. Jansson, I. J. Feain and B. M. Gaensler, **Galactic magnetic deflections and Centaurus A as a UHECR source**, *JCAP* **1301**, 023 (2013) doi:10.1088/1475-7516/2013/01/023 [arXiv:1211.7086 [astro-ph.HE]].
- [80] M. S. Sutherland, B. M. Baughman and J. J. Beatty, **CRT: A numerical tool for propagating ultrahigh energy cosmic rays through Galactic magnetic field models**, *Astropart. Phys.* **34**, 198 (2010) doi:10.1016/j.astropartphys.2010.07.002 [arXiv:1010.3172].
- [81] R. Smida and R. Engel, **The ultra-high energy cosmic rays image of Virgo A**, *PoS ICRC* **2015**, 470 (2016) doi:10.22323/1.236.0470 [arXiv:1509.09033 [astro-ph.HE]].
- [82] F. W. Stecker, J. F. Krizmanic, L. M. Barbier, E. Loh, J. W. Mitchell, P. Sokolsky and R. E. Streitmatter, **Observing the ultrahigh-energy universe with OWL eyes**, *Nucl. Phys. Proc. Suppl.* **136C**, 433 (2004) doi:10.1016/j.nuclphysbps.2004.10.027 [astro-ph/0408162].
- [83] A. Neronov, D. V. Semikoz, L. A. Anchordoqui, J. Adams and A. V. Olinto, **Sensitivity of a proposed space-based Cherenkov astrophysical-neutrino telescope**, *Phys. Rev. D* **95**, no. 2, 023004 (2017) doi:10.1103/PhysRevD.95.023004 [arXiv:1606.03629 [astro-ph.IM]].